

# Synthetic elastin hydrogels that are coblended with heparin display substantial swelling, increased porosity, and improved cell penetration

Yidong Tu,<sup>1</sup> Suzanne M. Mithieux,<sup>1</sup> Nasim Annabi,<sup>2</sup> Elizabeth A. Boughton,<sup>3</sup> Anthony S. Weiss<sup>1</sup>

<sup>1</sup>School of Molecular Bioscience, University of Sydney, NSW 2006, Australia

<sup>2</sup>School of Chemical and Biomolecular Engineering, University of Sydney, NSW 2006, Australia

<sup>3</sup>School of Aerospace, Mechatronic, and Mechanical Engineering, University of Sydney, NSW 2006, Australia

Received 18 February 2010; revised 29 June 2010; accepted 30 June 2010

Published online 11 October 2010 in Wiley Online Library (wileyonlinelibrary.com). DOI: 10.1002/jbm.a.32950

**Abstract:** Synthetic elastin hydrogels are useful tissue engineering scaffolds because they present cell binding sequences and display physical performance similar to that of human elastic tissue. Small pores and a low porosity can limit cellular penetration into elastin scaffolds. To overcome this problem, glycosaminoglycans were coblended with tropoelastin during the formation of synthetic elastin hydrogels. Heparin and dermatan sulfate increased the pore size and porosity of the hydrogels. Heparin was particularly effective as it enlarged the pore size from  $6.6 \pm 2.1 \mu\text{m}$  to  $23.8 \pm 8.5 \mu\text{m}$ , and generated structures occasionally separated by finely fenestrated thin walls, which allowed human dermal fibroblast cells to migrate as deep as  $\sim 300 \mu\text{m}$  into the hydrogel under diffusion-limiting static culture conditions. Most cells

displayed spindle-like morphology, appeared histologically normal and presented intact nuclei, as expected for a viable population. Hydrogel swelling studies showed that each of the hydrogels contracted as the temperature was raised from  $4^\circ\text{C}$  to  $37^\circ\text{C}$ ; synthetic elastin-heparin was least affected by temperature with a contraction of only  $22.4 \pm 1.2\%$ , which would facilitate its transition from cold storage to body temperature. All hydrogels displayed similar compression moduli of  $5.5 \pm 0.4$  to  $6.9 \pm 0.6$  kPa. Compressive elastic energy losses for synthetic elastin-heparin and synthetic elastin were  $33.7 \pm 1.3\%$  and  $31.7 \pm 2.2\%$  respectively. © 2010 Wiley Periodicals, Inc. *J Biomed Mater Res Part A*: 95A: 1215–1222, 2010.

**Key Words:** elastin, tropoelastin, glycosaminoglycan

## INTRODUCTION

Cell adhesion, differentiation, and infiltration are substantially influenced by tissue engineering scaffold microstructures that include porosity, pore size, shape, and interconnectivity,<sup>1–5</sup> and by the mechanical properties of the scaffold.<sup>6–11</sup> Elastin, collagen, and glycosaminoglycans (GAGs) are major components of the ECM and have been widely adopted as scaffold components<sup>12,13</sup> while collagen-GAG co-blend scaffolds are commercially used in dermal repair.<sup>14–24</sup>

The use of the dominant elastic ECM protein elastin has been limited in tissue engineering constructs because it is extremely insoluble as a consequence of extensive lysine mediated cross-links although this impediment has been partly removed through the use of chemically solubilized elastin.<sup>14,25</sup> The availability of recombinant forms of tropoelastin, the soluble precursor of elastin, has allowed for further research into the formation of tropoelastin-based scaffolds. Synthetic elastin scaffolds based on the polymerization of tropoelastin have strength, elasticity, and biocompatibility that approach that of human elastic tissue and are amenable to molding into a variety of shaped tissue substrata.<sup>26,27</sup> However, these synthetic elastin scaffolds are non-homogeneous and are enriched for small pores and display limited porosity, which limit cellular migration deep into the scaffolds.<sup>28</sup>

GAGs such as heparin and dermatan sulfate are complex polysaccharides that play important roles in cell growth, differentiation, morphogenesis, and cell migration.<sup>29–31</sup> GAGs have also been shown to promote tropoelastin self-assembly *in vitro* by binding tropoelastin through lysine side chains and lowering the critical concentration for the coacervation.<sup>32,33</sup> Mixed constructs of collagen, elastin, and GAGs have the potential to serve as versatile biomaterials.<sup>34</sup>

This study presents evidence that the pore size and connectivity of synthetic elastin scaffolds is improved by coblending with heparin and dermatan sulfate. The microstructure, pore morphology, swelling properties, and mechanical properties of these hydrogels demonstrate compressive elasticity and facilitate colonization by human dermal fibroblasts.

## MATERIALS AND METHODS

### Protein production and reagents

Recombinant human tropoelastin isoform SHELΔ26A (Synthetic Human Elastin without domain 26A) corresponding to amino acid residues 27–724 of GenBank entry AAC98394 (gi 182020) was purified as previously described.<sup>32</sup> Heparin (H3393) and dermatan sulfate (C3788-25MG) were from Sigma-Aldrich.

**Correspondence to:** A. S. Weiss; e-mail: anthony.weiss@sydney.edu.au  
Contract grant sponsors: Australian Research Council, The National Heart Foundation

### Hydrogel formation

Tropoelastin (100 mg/mL) was dissolved in phosphate-buffered saline (10 mM sodium phosphate pH 7.4, 150 mM sodium chloride; PBS) at 4°C. Cold heparin or dermatan sulfate was added from 4.2 to 16.7 mg/mL. Cold bis(sulfosuccinimidyl)suberate (BS3) solution was then added to 10 mM. Solutions were immediately transferred to 8-well glass slides (Lab-Tek chamber slide, Nalge Nunc International), and placed at 37°C for 16 h to facilitate coacervation and cross-linking.

### Scanning electron microscopy

Cross-linked elastin hydrogels were washed several times in PBS before being dehydrated three times in 50, 70, 80, 90, 95, and 100% (v/v) ethanol, each for 5 min. For drying, samples were soaked in 100% hexamethyldisilazane for 3 min and then transferred to a desiccator for at least 2 h. All samples were mounted on stubs, followed by coating in a Synvac Xenosput chromium coater for 150 s at 40 mA to give a thin (~3 nm) surface coating of chromium. Samples were examined using the Zeiss ultra plus FESEM with SE2 signal detector at 3–3.5 kV.

### Micro-CT analysis

Lyophilized elastin hydrogels were examined with a Skyscan 1072 high-resolution desktop X-ray CT scanner (Skyscan, Belgium). Samples were mounted on a plastic support that rotated vertically through 360°. The X-ray tube was set at 160 μA current and 60 kV voltage and samples were scanned with a 2.3-μm voxel resolution. 360° X-ray images of the samples were converted to 3D models using VG Studio Max software (Volume Graphics GmbH, Heidelberg, Germany).

### Swelling properties

The swelling behavior of elastin hydrogels was tested in PBS at 4, 20, and 37°C. All hydrogels were lyophilized and the masses of the dry hydrogels were recorded. Samples were hydrated at 4°C and then swelled in PBS at the specified temperatures for 20 h. Excess PBS was removed from each of the samples and the swelling ratio was calculated based on a ratio of the increase in mass to that of the dry sample, verified by assessment of the amount of expelled PBS. For each type of hydrogel, at least three samples were tested.

### Mechanical properties

Uniaxial compression tests were performed in an unconfined state using a Bose ELF3400 mechanical tester with a 50 N load cell. The testing procedure was as described previously.<sup>28,35–37</sup> Prior to mechanical testing, the hydrogels were swelled for 5 h in PBS. The compressive properties of the samples were tested in the hydrated state, in PBS, at room temperature. Compression (mm) and load (N) were recorded using Wintest software at a cross speed of 30 μm/s and 50% strain level. Samples were cyclically preconditioned for seven cycles. The hydrogels were subsequently subjected to another loading and unloading cycle (8th cycle) where compression (mm) and load (N) were collected. The compressive modulus for the 8th cycle was obtained using

linear regression between strains of 0–0.2 mm/mm. In addition, the energy loss based on the 8th compression cycle was calculated using the following formula:

$$\text{Energy loss} = 100\% \times (\text{area under loading curve} - \text{area under unloading curve}) / \text{area under loading curve}.$$

At least three specimens were tested for each type of hydrogel.<sup>38–40</sup>

### *In vitro* cell culture

Hydrogels in 24-well plates were sterilized by soaking three times with ethanol followed by three washes in culture media (DMEM, 10%FBS, pen-strep) then equilibrated in culture media at 37°C for 16 h. Human dermal fibroblasts (GM3348, Coriell Research Institute, NJ) were seeded onto the hydrogels at  $2 \times 10^5$  cells per well and were cultured in a CO<sub>2</sub> incubator for to days at 37°C. Samples were fixed with 2.5% glutaraldehyde in 0.1M phosphate buffer pH 7.2 (PB) for 1 h and 1% osmium in 0.1M PB for 1 h, then dehydrated and analyzed by SEM.

### Histology staining and light microscopy analysis

Following *in vitro* cell culture, hydrogels were fixed in 10% formalin and dehydrated through a graded series of ethanol and xylene solvents, then embedded in paraffin wax. Five micron-thick sections were cut and dried on glass slides, then deparaffinized and rehydrated. Cross-sections were stained with hematoxylin & eosin.

## RESULTS

### Synthetic elastin-GAG hydrogels

Totally, 100 mg/mL tropoelastin and 10 mM BS3 were dissolved in cold PBS then placed at 37°C for 16 h to facilitate coacervation and cross-linking. The solution formed slightly yellow elastic hydrogels similar to those described previously.<sup>26–27</sup> Comparable hydrogels were formed when 4.17, 8.35, and 16.7 mg/mL heparin or when 8.35 mg/mL dermatan sulfate co-blended at 37°C with 100 mg/mL tropoelastin solutions. However if the concentration of dermatan sulfate was increased to 16.7 mg/mL, a concentrated thin product was formed that was soft, inelastic, and fragile.

Two milliliter 100 mg/mL tropoelastin and 10 mM BS3 in PBS and 2 mL 100 mg/mL tropoelastin, 10 mM BS3, and 16.7 mg/mL heparin in PBS were separately transferred into 3-mL syringes (Terumo Corporation). Hydrogels formed inside the syringes after incubation at 37°C for 16 h. The tropoelastin solution formed a compact hydrogel at the bottom of the syringe that was ~25% of the volume of the starting solution; in contrast, the tropoelastin-heparin solution gave a larger, porous cylindrical hydrogel that was ~80% the volume of the starting solution [Fig. 1(A)]. These structures retained their shape after removal from the syringes [Fig. 1(B)].

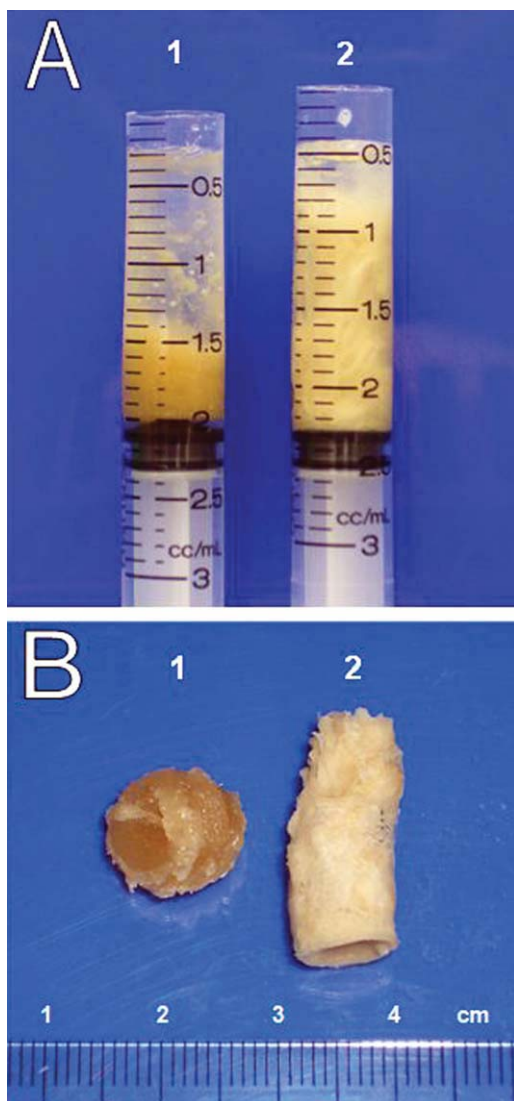


**FIGURE 1.** Visual comparisons of hydrogels made using (#1) 100 mg/mL tropoelastin and (#2) 100 mg/mL tropoelastin co-blended with 16.7 mg/mL heparin, (A) inside syringes, (B) after removing from the syringes. [Color figure can be viewed in the online issue, which is available at [wileyonlinelibrary.com](http://wileyonlinelibrary.com).]

### Structure of synthetic elastin hydrogels

The tropoelastin-based hydrogel (SE) was analyzed by SEM. Both the top surface [Fig. 2(A)] and the cross-section [Fig. 2(B)] of the hydrogel displayed a compact structure with small ( $6.6 \pm 2.1 \mu\text{m}$ ) isolated pores.

The hydrogel that was made using 100 mg/mL tropoelastin and 16.7 mg/mL heparin differed from SE in that it was composed of two parts: a 100  $\mu\text{m}$  thick outer region [Fig. 2(C)] with  $\sim 2\text{--}5 \mu\text{m}$  diameter pores [Fig. 2(D)], and an inner region that consisted of  $23.8 \pm 8.5 \mu\text{m}$  pores ( $n = 100$ ). This  $\sim 100 \mu\text{m}$  thick outer region was removed before seeding cells. The pores of the inner region had thin walls that were connected by small fenestrations [Fig. 2(E)]. Similar structures were seen when the 100 mg/mL tropoelastin solution contained either 8.35 or 4.17 mg/mL of heparin [Fig. 2(F,G)]. Dermatan sulfate had only a small effect on the

hydrogel structure: with 100 mg/mL tropoelastin and 8.35 mg/mL dermatan sulfate the pore size ( $n = 100$ ) was only  $14.1 \pm 4.2 \mu\text{m}$  [Fig. 2(H)] which was too small for cells to penetrate.

Different concentrations of heparin had a similar effect on the hydrogel structure; hydrogels made using higher concentrations of heparin had a regular shape with pores that were of a more uniform size and shape. Only the 8.35 mg/mL dermatan sulfate was able to form a co-blended hydrogel. On this basis, subsequent constructs were made with 100 mg/mL tropoelastin and 16.7 mg/mL heparin (SE-Hep) and 100 mg/mL tropoelastin and 8.35 mg/mL dermatan sulfate (SE-DS).

### Three-dimensional models of synthetic elastin hydrogels

Micro-CT facilitated a deeper 3D description of the hydrogel structures than could be obtained by SEM. SE displayed many small pores [Fig. 3(A)]. By visual assessment, SE-Hep [Fig. 3(B)] and SE-DS [Fig. 3(C)] presented increased porosity than compared to SE. Apparent sizes compared with those seen in SEM.

### The swelling ratios for synthetic elastin hydrogels at different temperatures

The swelling ratios of SE, SE-Hep, and SE-DS hydrogels are shown in Figure 4. These ratios were used to compare the contraction of the hydrogel in the transition from  $4^\circ\text{C}$  to  $37^\circ\text{C}$  (Table I). All hydrogels expelled PBS as the temperature rose. SE showed the most substantial change as its swelling ratio decreased  $62.8 \pm 4.8\%$  over this temperature range. SE-DS was intermediate with a decrease of  $31.1 \pm 2.8\%$ . SE-Hep was the least affected by temperature with a swelling ratio decrease of only  $22.4 \pm 1.2\%$ .

### Mechanical properties of synthetic elastin hydrogels

Compression tests were performed on PBS-hydrated SE, SE-Hep and SE-DS at room temperature and subjected to *t*-test analysis (two-sample assuming unequal variances) in order to determine statistical significance. SE-Hep was more elastic than either SE-DS or SE. The compression moduli for SE, SE-Hep, and SE-DS hydrogels were  $6.9 \pm 0.57$ ,  $5.5 \pm 0.42$ , and  $6.2 \pm 1.58 \text{ kPa}$  respectively over 0–0.2 mm/mm strain. SE-DS displayed the highest energy loss of  $41.5 \pm 1.5\%$ , while lower energy loss was observed on SE and SE-Hep as  $31.7 \pm 2.2\%$  and  $33.7 \pm 1.3\%$  (Table II).

### *In vitro* cell proliferation and penetration on synthetic elastin-GAG hydrogels

Human dermal fibroblasts were seeded onto SE-Hep and SE-DS. Histology staining showed that fibroblasts had proliferated on the SE-Hep surface and penetrated ( $\sim 300 \mu\text{m}$ ) into the hydrogel over two days [Fig. 5(A)]. About half of the cells penetrated into the hydrogels and  $\sim 10\%$  of all cells migrated as deep as  $300 \mu\text{m}$ . Most cells displayed spindle-like morphology, appeared histologically normal and presented intact nuclei, as expected for a viable population. Over a longer period of time *in vitro*, cells continue to colonize the

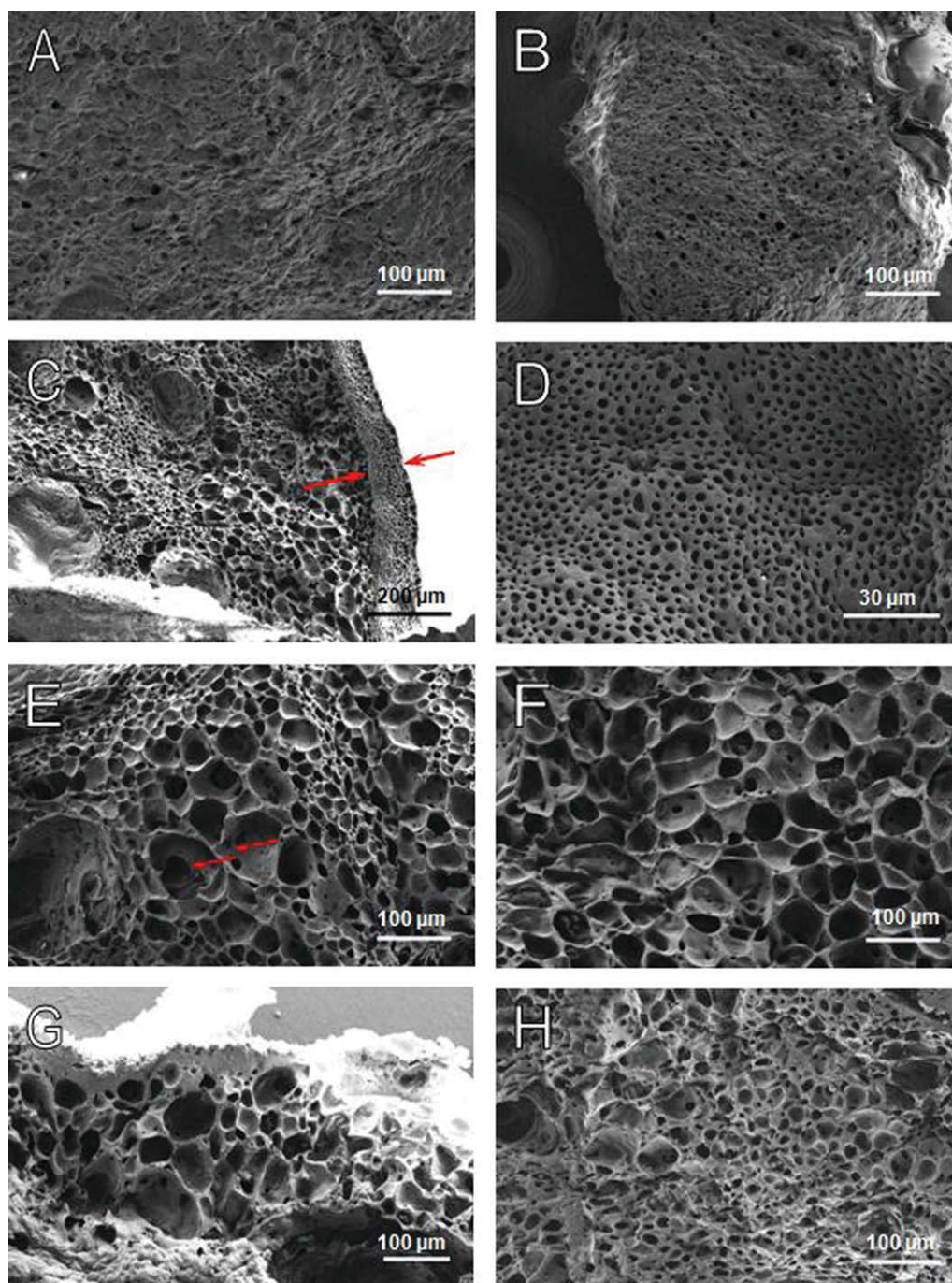


**FIGURE 2.** SEM images of the (A) surface and (B) cross-section of a synthetic elastin hydrogel, (C) thin outer layer as indicated by arrows and (D) top surface of a synthetic elastin hydrogel containing 16.7 mg/mL heparin, (E) cross-section of synthetic elastin hydrogels containing 16.7 mg/mL heparin; thin fenestrations are as indicated by arrows, (F) 8.35 mg/mL heparin, (G) 4.17 mg/mL heparin, and (H) 8.35 mg/mL dermatan sulfate. [Color figure can be viewed in the online issue, which is available at [wileyonlinelibrary.com](http://wileyonlinelibrary.com).]

matrix but did not penetrate below  $\sim 300 \mu\text{m}$ . We would not have expected and did not see further penetration under static growth conditions as beyond this depth cells are no longer viable due to limitations on gas and nutrient diffusion. Without using an intrinsic capillary network, the maximum penetration of cells is approximately 150–200  $\mu\text{m}$  because of the lack of oxygen within the deeper compartments of the biomaterial.<sup>41</sup>

Cells had attached to and occasionally penetrated the thin interstitial walls between the pores [Fig. 5(B)]. SEM analysis confirmed that cells had spread on the hydrogel surfaces and migrated into pores [Fig. 5(C,D)]. For SE-DS, histology staining and SEM analysis revealed a monolayer of cells on the hydrogel surface; few cells had penetrated presumably due to the smaller pore sizes and thicker walls between the pores [Fig. 6(A,B)].

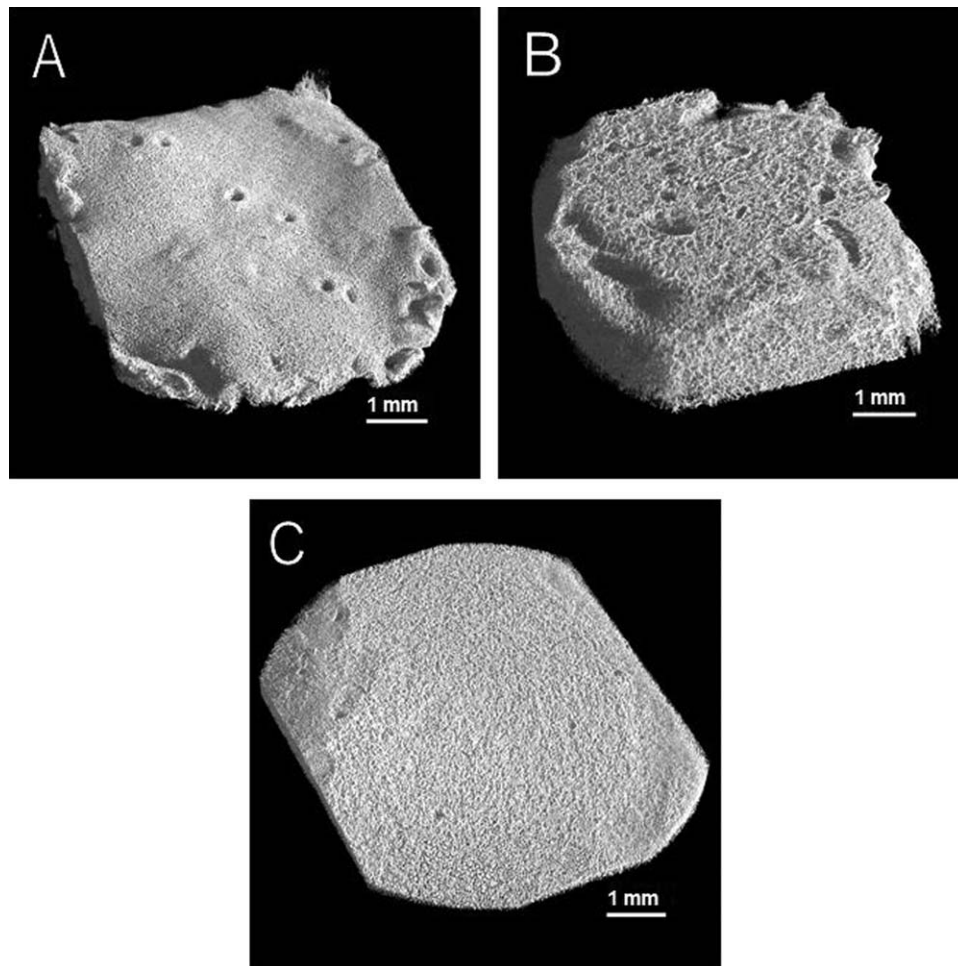


FIGURE 3. Micro-CT images of (A) SE hydrogel, (B) SE-Hep hydrogel, and (C) SE-DS hydrogel.

## DISCUSSION

In this study, two types of GAG were introduced into synthetic elastin hydrogel formations to increase their pore size and penetration. Heparin had a substantial effect on the microstructure of synthetic elastin hydrogels. The pore sizes of SE-Hep were  $\sim 3.6$ -fold large than in SE hydrogels, and

their pores appeared to be connected by small holes that penetrated their thin walls. Dermatan sulfate had a smaller effect, with at most a doubling in pore size seen for SE-DS. Porosity was tolerant of variations in heparin concentration, pointing to a titration with tropoelastin, beyond which the GAG had little additional effect. We speculate that these GAG effects were due to a combination of increased solution viscosity<sup>42,43</sup> and the reorganizing ability of GAGs to perturb and promote tropoelastin assembly.<sup>32</sup>

Changes in the swelling ratio of SE-GAG were considerably less than those seen for SE hydrogels. This was especially seen for SE-Hep hydrogels, which changed little ( $22.4 \pm 1.2\%$ ) in the transition from  $4^\circ\text{C}$  to  $37^\circ\text{C}$ , in contrast to SE hydrogels which contracted by  $62.8 \pm 4.8\%$  that is they contracted to almost one-third of their original size. This

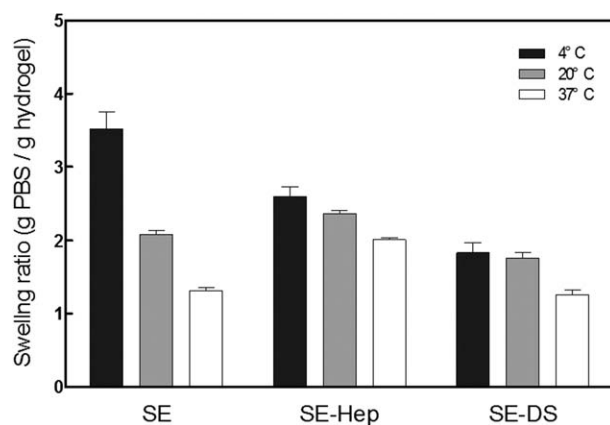


FIGURE 4. Swelling ratios for each type of the synthetic elastin hydrogels at various temperatures.

TABLE I. Temperature Dependence of Buffer Retention by Each Hydrogel (g PBS per g Hydrogel)

	SE-Hep	SE-DS	SE
$4^\circ\text{C}$	$2.59 \pm 0.14$	$1.83 \pm 0.14$	$3.52 \pm 0.23$
$20^\circ\text{C}$	$2.36 \pm 0.04$	$1.76 \pm 0.07$	$2.08 \pm 0.06$
$37^\circ\text{C}$	$2.01 \pm 0.03$	$1.26 \pm 0.06$	$1.31 \pm 0.05$

**TABLE II. Compressive Modulus and Percentage of Energy Loss for Elastin Hydrogel Constructs**

	Compressive Modulus (kPa)	Energy Loss (%)
SE	6.9 ± 0.57	31.7 ± 2.2
SE-Hep	5.5 ± 0.42	33.7 ± 1.3
SE-DS	6.2 ± 1.58	41.5 ± 1.5

change of properties is likely to be due to contributions by salt bridges that assist in constraining the structure of SE-GAG hydrogels.<sup>7</sup> Control over temperature dependent swelling could be quite beneficial for surgical applications given their physical adaptability as the biomaterials are taken from cold storage to body temperature. As temperature-dependent responses in elastin-based hydrogels reflect extensional flexibility in the protein chains, we infer that the tropoelastin polypeptides in these SE-GAG constructs are more constrained than in synthetic elastin hydrogels. Cell penetration, survival and proliferation studies were conducted at 37°C and it would be interesting to conduct a detailed study of the material under strain at 20°C and 37°C using a variable strain bioreactor system. This study focused on energy losses, not differences in the compression moduli of fabricated hydrogels. There was a significant difference between the energy losses of SE-DS and SE-Hep, and those of SE-DS

and SE. Energy loss is proportional to hysteresis and a greater energy loss means a less elastic nature.<sup>1</sup> SE-DS displayed more hysteresis than SE-Hep and SE. The compression modulus of SE-Hep was slightly lower than SE-DS and SE hydrogels confirming that SE-Hep was more porous than the other two types of hydrogels. Comparable compression elasticity was obtained for each of the hydrogels which confirmed that SE-GAG hydrogels retained the compression properties of SE hydrogels. The energy loss of SE-Hep was 1.4 fold higher than that of purified native elastin reported to be 23 ± 10%.<sup>39</sup>

One of the most important functions of tissue engineering scaffolds is to provide a framework and initial support for the cells to attach, proliferate, and penetrate.<sup>44</sup> Scaffolds used for dermal repair are inactive when the mean pore size is either lower than 20 μm or higher than about 120 μm although these values can vary with scaffold type and incubation conditions.<sup>45</sup> SE hydrogels have nonhomogeneous small pores, which collectively limit deep cell migration.<sup>26</sup> Human dermal fibroblasts either spread only on the SE hydrogel surface or grew slightly into the SE hydrogel (<30 μm) after 14 days' incubation.<sup>28</sup> The transition to SE-Hep was substantial because it increased pore size and penetration to enable dermal fibroblast infiltration to ~300 μm in two days. Additionally, the finely fenestrated, diaphanous

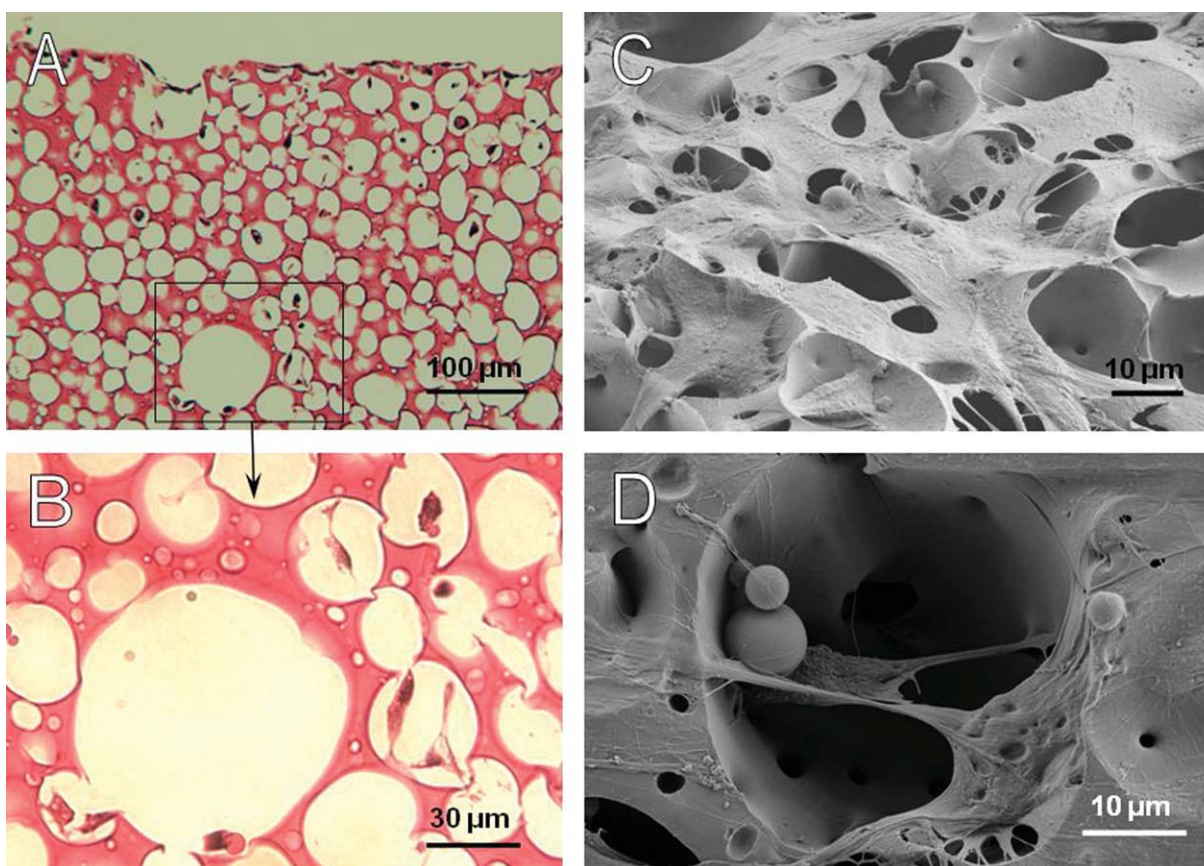


**FIGURE 5.** Histology images of hematoxylin and eosin stained sections of (A) SE-Hep hydrogels with fibroblast cells showing cells within the scaffold, (B) magnification of a section of the previous panel; (C) SEM showing fibroblasts on SE-Hep; and (D) fibroblasts bridging and penetrating a pore. [Color figure can be viewed in the online issue, which is available at [wileyonlinelibrary.com](http://wileyonlinelibrary.com).]

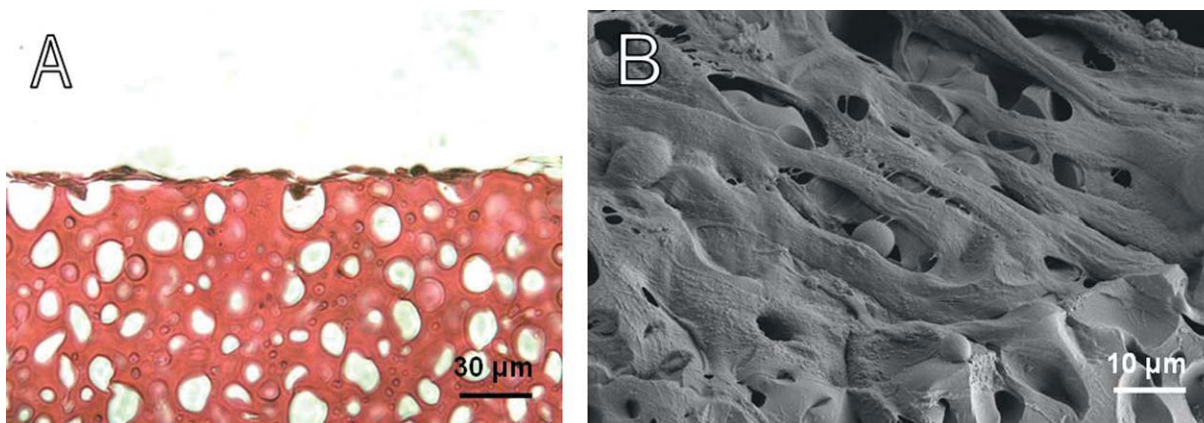


**FIGURE 6.** (A) Histology image of hematoxylin and eosin stained section of SE-DS showing fibroblasts surface monolayer growth. (B) SEM showing fibroblasts on the surface of SE-DS. [Color figure can be viewed in the online issue, which is available at [wileyonlinelibrary.com](http://wileyonlinelibrary.com).]

walls of these pores might have allowed for proteolytically mediated cell migration.

### CONCLUSION

In this study, GAGs were coblend into synthetic elastin hydrogels to increase their porosity. Heparin was found to have a substantial effect on hydrogel structure formation with pore sizes increasing from  $6.6 \pm 2.1 \mu\text{m}$  to  $23.8 \pm 8.5 \mu\text{m}$ . These larger and deeper pores allowed human dermal fibroblasts to migrate further into the hydrogel. SE-Hep had similar mechanical properties to, but displayed less swelling than, SE hydrogels. These appropriate mechanical and biological properties indicate that SE-Hep is an improvement over SE and that it can be contemplated as an elastic biomaterial for cell-interactive applications such as dermal repair.

### ACKNOWLEDGMENTS

The authors acknowledge the facilities as well as scientific and technical assistance from staff in the AMMRF (Australian Microscopy and Microanalysis Research Facility) at the Electron Microscope Unit, The University of Sydney. They also wish to thank Sarah Martinez for technical assistance.

### REFERENCES

- Annabi N, Mithieux SM, Weiss AS, Dehghani F. The fabrication of elastin-based hydrogels using high pressure CO<sub>2</sub>. *Biomaterials* 2009;30:1–7.
- Nehrer S, Breinan HA, Ramappa A, Young G, Shortkroff S, Louie LK, Sledge CB, Yannas IV, Spector M. Matrix collagen type and pore size influence behaviour of seeded canine chondrocytes. *Biomaterials* 1997;18:769–776.
- Wake MC, Patrick CW Jr, Mikos AG. Pore morphology effects on the fibrovascular tissue growth in porous polymer substrates. *Cell Transplant* 1994;3:339–343.
- O'Brien FJ, Harley BA, Yannas IV, Gibson LJ. The effect of pore size on cell adhesion in collagen-GAG scaffolds. *Biomaterials* 2005;26:433–441.
- Zeltinger J, Sherwood JK, Graham DA, Mueller R, Griffith LG. Effect of pore size and void fraction on cellular adhesion, proliferation, and matrix deposition. *Tissue Eng* 2001;7:557–572.
- Freyman TM, Yannas IV, Yokoo R, Gibson LJ. Fibroblast contraction of a collagen-GAG matrix. *Biomaterials* 2001;22:2883–2891.
- Annabi N, Mithieux SM, Boughton EA, Ruys AJ, Weiss AS, Dehghani F. Synthesis of highly porous crosslinked elastin hydrogels and their interaction with fibroblasts in vitro. *Biomaterials* 2009;30:4550–4557.
- Zaman MH, Trapani LM, Sieminski AL, Mackellar D, Gong H, Kamm RD, Wells A, Lauffenburger DA, Matsudaira P. Migration of tumor cells in 3D matrices is governed by matrix stiffness along with cell-matrix adhesion and proteolysis. *Proc Natl Acad Sci USA* 2006;103:10889–10894.
- Peyton SR, Putnam AJ. Extracellular matrix rigidity governs smooth muscle cell motility in a biphasic fashion. *J Cell Physiol* 2005;204:198–209.
- Jiang H, Grinnell F. Cell-matrix entanglement and mechanical anchorage of fibroblasts in three-dimensional collagen matrices. *Mol Biol Cell* 2005;16:5070–5076.
- Yeung T, Georges PC, Flanagan LA, Marg B, Ortiz M, Funaki M, Zahir N, Ming W, Weaver V, Janmey PA. Effects of substrate stiffness on cell morphology, cytoskeletal structure, and adhesion. *Cell Motil Cytoskeleton* 2005;60:24–34.
- Lee CH, Singla A, Lee Y. Biomedical applications of collagen. *Int J Pharm* 2001;221(1–2):1–22.
- Liu C, Xia Z, Czernuszka JT. Design and development of three-dimensional scaffolds for tissue engineering. *Chem Eng Res Des* 2007;85(A7):1051–1064.
- Daamen WF, van Moerkerk HT, Hafmans T, Buttafoco L, Poot AA, Veerkamp JH, van Kuppevelt TH. Preparation and evaluation of molecularly-defined collagen-elastin-glycosaminoglycan scaffolds for tissue engineering. *Biomaterials* 2003;24:4001–4009.
- Torres DS, Freyman TM, Yannas IV, Spector M. Tendon cell contraction of collagen-GAG matrices in vitro: Effect of cross-linking. *Biomaterials* 2000;21:1607–1619.
- Harley BA, Leung JH, Silva EC, Gibson LJ. Mechanical characterization of collagen-glycosaminoglycan scaffolds. *Acta Biomater* 2007;3:463–474.
- Zaleskas JM, Kinner B, Freyman TM, Yannas IV, Gibson LJ, Spector M. Growth factor regulation of smooth muscle actin expression and contraction of human articular chondrocytes and meniscal cells in a collagen-GAG matrix. *Exp Cell Res* 2001;270:21–31.
- Orgill DP, Straus FH II, Lee RC. The use of collagen-GAG membranes in reconstructive surgery. *Ann NY Acad Sci* 1999;888:233–248.
- Stiefel D, Schiestl CM, Meuli M. The positive effect of negative pressure: Vacuum-assisted fixation of Integra artificial skin for reconstructive surgery. *J Pediatr Surg* 2009;44:575–580.
- Palao R, Gomez P, Huguet P. Burned breast reconstructive surgery with Integra dermal regeneration template. *Br J Plast Surg* 2003;56:252–259.
- Lee LF, Porch JV, Spenler W, Garner WL. Integra in lower extremity reconstruction after burn injury. *Plast Reconstr Surg* 2008;121:1256–1262.
- Fitton AR, Drew P, Dickson WA. The use of a bilaminate artificial skin substitute (Integra) in acute resurfacing of burns: An early experience. *Br J Plast Surg* 2001;54:208–212.

23. Jones I, Currie L, Martin R. A guide to biological skin substitutes. *Br J Plast Surg* 2002;55:185–193.
24. Winfrey ME, Cochran M, Hegarty MT. A new technology in burn therapy: INTEGRA artificial skin. *Dimens Crit Care Nurs* 1999;18:14–20.
25. Daamen WF, Veerkamp JH, van Hest JC, van Kuppevelt TH. Elastin as a biomaterial for tissue engineering. *Biomaterials* 2007;28:4378–4398.
26. Mithieux SM, Rasko JE, Weiss AS. Synthetic elastin hydrogels derived from massive elastic assemblies of self-organized human protein monomers. *Biomaterials* 2004;25:4921–4927.
27. Mithieux SM, Wise SG, Raftery MJ, Starcher B, Weiss AS. A elastin two-component system for studying the architecture of elastin assembly in vitro. *J Struct Biol* 2005;149:282–289.
28. Rnjak J, Li Z, Maitz PMM, Wise SG, Weiss AS. Primary human dermal fibroblast interactions with open weave three-dimensional scaffolds prepared from synthetic human elastin. *Biomaterials* 2009;30:6469–6477.
29. Yamada S, Sugahara K. Potential therapeutic application of chondroitin sulfate/dermatan sulfate. *Curr Drug Discov Technol* 2008;5:289–301.
30. Capila I, Linhardt RJ. Heparin-protein interactions. *Angew Chem Int Ed Engl* 2002;41:391–412.
31. Casu B, Lindahl U. Structure and biological interactions of heparin and heparan sulfate. *Adv Carbohydr Chem Biochem* 2001;57:159–206.
32. Wu WJ, Vrhovski B, Weiss AS. Glycosaminoglycans mediate the coacervation of human tropoelastin through dominant charge interactions involving lysine side chains. *J Biol Chem* 1999;274:21719–21724.
33. Tu Y, Weiss AS. Glycosaminoglycan-mediated coacervation of tropoelastin abolishes the critical concentration, accelerates coacervate formation, and facilitates spherule fusion: Implications for tropoelastin microassembly. *Biomacromolecules* 2008;9:1739–1744.
34. Geutjes PJ, Daamen WF, Buma P, Feitz WF, Faraj KA, van Kuppevelt TH. From molecules to matrix: Construction and evaluation of molecularly defined bioscaffolds. *Adv Exp Med Biol* 2006;585:279–295.
35. Srokowski EM, Woodhouse KA. Development and characterisation of novel cross-linked bio-elastomeric materials. *J Biomater Sci Polym Ed* 2008;19:785–799.
36. Stammen JA, Williams S, Ku DN, Guldberg RE. Mechanical properties of a novel PVA hydrogel in shear and unconfined compression. *Biomaterials* 2001;22:799–806.
37. Joshi A, Fussell G, Thomas J, Hsuan A, Lowman A, Karduna A, Vresilovic E, Marcolongo M. Functional compressive mechanics of a PVA/PVP nucleus pulposus replacement. *Biomaterials* 2006;27:176–184.
38. Srokowski EM, Woodhouse KA. Development and characterisation of novel cross-linked bio-elastomeric materials. *J Biomater Sci Polym Ed* 2008;19:785–799.
39. Bellingham CM, Lillie MA, Gosline JM, Wright GM, Starcher BC, Bailey AJ, Woodhouse KA, Keeley FW. Recombinant human elastin polypeptides self-assemble into biomaterials with elastin-like properties. *Biopolymers* 2003;70:445–455.
40. Vieth S, Bellingham CM, Keeley FW, Hodge SM, Rousseau D. Microstructural and tensile properties of elastin-based polypeptides crosslinked with genipin and pyrroloquinoline quinone. *Biopolymers* 2007;85:199–206.
41. Fidkowski C, Kaazempur-Mofrad MR, Borenstein J, Vacanti JP, Langer R, Wang Y. Endothelialized microvasculature based on a biodegradable elastomer. *Tissue Eng* 2005;11(1–2):302–309.
42. Voet D, Voet JG, Pratt CW. *Fundamentals of Biochemistry*. New York: Wiley; 1999.
43. Ruponen M, Ronkko S, Honkakoski P, Pelkonen J, Tammi M, Urtti A. Extracellular glycosaminoglycans modify cellular trafficking of lipoplexes and polyplexes. *J Biol Chem* 2001;276:33875–33880.
44. Sachlos E, Czernuszka JT. Making tissue engineering scaffolds work. Review: The application of solid freeform fabrication technology to the production of tissue engineering scaffolds. *Eur Cell Mater* 2003;5:29–39;discussion 39–40.
45. Yannas IV, Lee E, Orgill DP, Skrabut EM, Murphy GF. Synthesis and characterization of a model extracellular matrix that induces partial regeneration of adult mammalian skin. *Proc Natl Acad Sci USA* 1989;86:933–937.